
Quantitative FWI characterization and monitoring of reservoir properties at the CMC Newell County Facility

Qi Hu, Matt Eaid, Scott Keating, and Kristopher A. Innanen

ABSTRACT

The spatial distribution of CO₂ saturation and the plume location can be monitored using time-lapse seismic data. Due to the limited knowledge of rock and fluid properties before injection, model predictions are often uncertain and must be updated when new measurements are available. The 2018 CMC VSP survey provided a dataset suitable for creating a baseline subsurface model for later monitoring studies. In this report, we apply full waveform inversion to the measured data, to reconstruct the subsurface model of elastic and rock physics properties. The key strategies used in our FWI framework are the effective source method for coping with near surface complexity, the inclusion of DAS data in FWI for leveraging the complementary aspects of accelerometer and DAS data, and the rock physics parameterized FWI that allows for jointly updating the elastic and rock physics variables. The result is high-resolution, plausible, and has a good agreement with the well-log data.

INTRODUCTION

The Carbon Management Canada (CMC) Newell County Facility is a platform for development and performance validation of technologies intended for measurement, monitoring and verification of CO₂ storage (Lawton et al., 2017). In 2018, a vertical seismic profile (VSP) baseline survey was acquired using accelerometers and collocated distributed acoustic sensing (DAS) fiber in a monitoring well located approximately 20 meters southwest of the injector well. The subsurface models obtained from this survey can be used to support further time-lapse analysis, e.g., reduce the uncertainty in predicting CO₂ distribution during injection and migration. In this report, we focus on using the technology of full-waveform inversion (FWI) to reconstruct elastic and reservoir property models from the measured data.

Prior to its inclusion in FWI, the field data must be processed to make them more comparable to simulated data generated by modeling procedures and to remove artifacts from the data. The processing workflow performed on each of the accelerometer and DAS datasets is detailed in (Eaid et al., 2021a). Figure 1 plots the processed datasets for several shot points on source line 1. In addition to seismic data, a comprehensive log suite was acquired at the injection well. The wireline logs were further interpreted that provides depth profiles of porosity and mineral composition. Hu et al. (2022b) construct a rock physics model combining the soft-sand model and Gassmann's equations to link the elastic and rock property logs. The model predicts the data accurately, then is used to reconstruct the shallow section of the velocity and density logs (Figure 2).

The preliminary FWI results for this survey are given in Keating et al. (2021) using accelerometer data and Eaid et al. (2021b) using both DAS and hybrid DAS-accelerometer data subsets. Two of the strategies they promote to improve the convergence are the ef-

fective source method for addressing near surface complexity and the log-derived single-parameter inversion for preventing parameter crosstalk. Eaid et al. (2021b) also illustrate that inverting both accelerometer and DAS data together has a stabilizing effect on the inverted models when compared to using either dataset alone. While using the single-parameter inversion offers advantages, it also causes a loss of elasticity information in the result that is important for reservoir property characterization. In addition, the assumption made for this parameterization, namely the model variables such as velocity and density are perfectly correlated, introduces uncertainty to the inversion. In this work, while retaining most of the existing strategies, we extend the FWI framework to three-parameter elastic inversion and direct rock physics parameter inversion (Hu et al., 2021).

In this work, we perform 2D frequency-domain isotropic-elastic FWI on the 2018 CMC VSP dataset including both accelerometer and DAS measurements. We first review the key FWI strategies we apply to the field data, including the effective source method, the inclusion of DAS data in FWI, and the FWI framework which allows for direct updating of rock properties. We then propose two workflows combining FWI and rock physics for the prediction of both elastic and rock physics properties in the field. One is a conventional workflow, where we first estimate the elastic properties using FWI, then invert these elastic properties for rock physics properties using a Bayesian approach. The other is a direct approach, in which we estimate the rock properties directly from seismic data, the corresponding elastic properties are then jointly output.

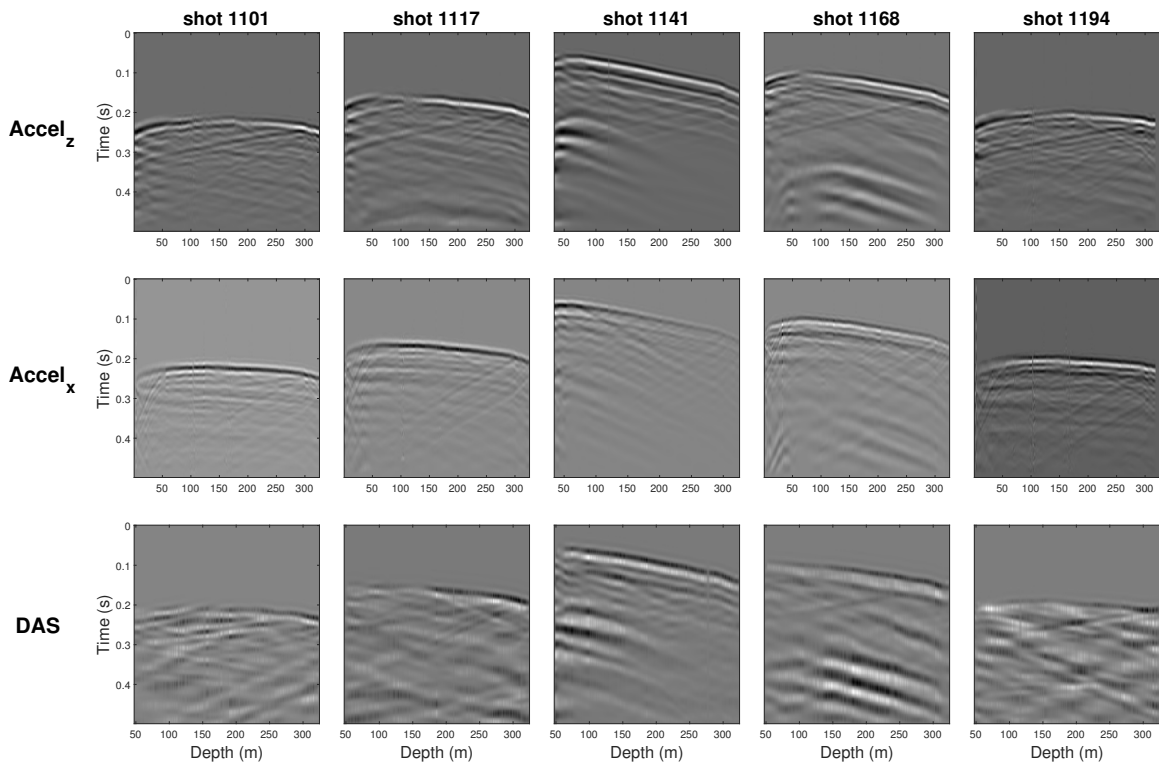


FIG. 1. Processed accelerometer and DAS data for the shot points on source line 1 (Eaid et al., 2021a).

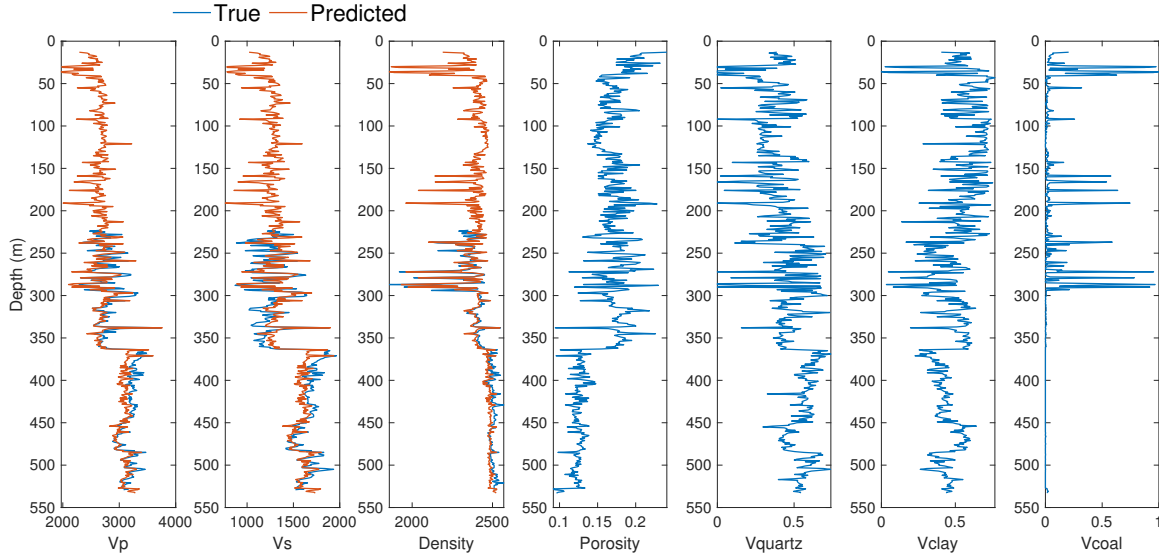


FIG. 2. Well-log data of the injection well: P-wave velocity, S-wave velocity, density, porosity, and the volume fractions of quartz, clay, and coal. The blue and red curves denote the real data and the data predicted by the rock physics model (Hu et al., 2022b).

THEORY

In FWI, the inverse problem is generally framed as an attempt to minimize the data misfit, subject to an assumed wave propagation model linking the wavefield and subsurface together. The objective function can be written as

$$E(\mathbf{m}) = \frac{1}{2} \|\mathbf{R}\mathbf{u} - \mathbf{d}\|_2^2 \quad \text{subject to} \quad \mathbf{A}(\mathbf{m})\mathbf{u} = \mathbf{f}, \quad (1)$$

where \mathbf{R} is the sampling matrix representing receiver measurement, \mathbf{u} is the displacement wavefield simulated from model vector \mathbf{m} , \mathbf{d} is the measured data, \mathbf{A} is a finite-difference forward modeling operator, and \mathbf{f} is the source term. Within a Newton optimization, the search direction $\delta\mathbf{m}$ for model update is the solution of

$$\mathbf{H} \delta\mathbf{m} = -\nabla_{\mathbf{m}}E, \quad (2)$$

where $\nabla_{\mathbf{m}}E$ and \mathbf{H} are the gradient and the Hessian of the objective function, respectively. We employ the l -BFGS method, which stores the changes of the gradient and model from a limited number of previous iterations and uses the stored information to approximate the inverse of the Hessian (Nocedal and Wright, 1999).

Effective source estimation

Keating et al. (2021) propose a strategy for FWI of VSP data sets where the effects of the near-surface are significant. In this approach, they eliminate the need to characterize the near-surface by replacing each surface source used in the data acquisition with an effective source at depth. Unlike unconventional formulations of FWI where only the subsurface model \mathbf{m} is treated as unknown in the inversion, they introduce an additional unknown \mathbf{a}

variable characterizing the wavefield after propagation through the near surface. Equation 1 is rewritten as

$$E(\mathbf{m}, \mathbf{f}^*) = \frac{1}{2} \|\mathbf{R}\mathbf{u} - \mathbf{d}\|_2^2 \quad \text{subject to} \quad \mathbf{A}(\mathbf{m})\mathbf{u} = \mathbf{f}^*, \quad (3)$$

Equation 3 is effectively the same optimization problem as conventional FWI, with the exception that we define the problem on a smaller model domain, and we invert for both an unknown model \mathbf{m} and an unknown source term \mathbf{f}^* . The details of simultaneous FWI prediction of model and source properties, such as the expressions for gradient and Hessian-vector product, are presented in Keating and Innanen (2020).

Inclusion of DAS data in FWI

The strain field associated with the displacements in Equation 1 is

$$\epsilon_{ij} = \frac{1}{2} \left(\frac{\partial u_i}{\partial x_j} + \frac{\partial u_j}{\partial x_i} \right), \quad (i, j) \text{ ranging over } (x, y, z), \quad (4)$$

In practice, the strain tensors in equation 4 are solved on a grid that is staggered relative to that of the displacements (Eaid et al., 2020). To generate a model of the local DAS fiber response, the strain tensors in the field coordinate system (x, y, z) must be transformed into the local system describing the fiber, from which the tangential tensor is extracted.

The inclusion of DAS data in FWI requires an objective function that can compare observed and modeled strain sampled along the tangent of a fiber embedded in the sub-surface. The matrix \mathbf{R} in Equation 1, which acts to sample the displacement wavefield, can be understood more generally as an operator that transforms the output of the numerical simulation of the wavefield into quantities that are directly comparable to the observed data. This allows us to use any standard FWI algorithm by simply reformulating the wavefield sampling matrix \mathbf{R} . Specifically, when incorporating DAS data, \mathbf{R} is responsible for computing the strain field along the DAS fiber, applying gauge length averaging, and computing the tangential strain for each receiver location along the fiber. These steps are given in detail in Eaid et al. (2020).

Rock physics parameterized FWI

Hu et al. (2021) formulated a direct procedure for updating rock and fluid properties within elastic FWI. This was achieved by re-parameterizing the inversion in terms of rock physics properties, adopting a viewpoint similar to that of Russell et al. (2011) within an AVO environment.

Let $\mathbf{m} = [m^1, m^2, m^3]$ represent a reference FWI parameterization which is based on three elastic parameters (e.g., the P- and S-wave velocities plus density) and $\mathbf{r} = [r^1, r^2, \dots, r^n]$ represent a desired FWI parameterization based on n different rock physics properties, we can express the elastic variables at the i^{th} spatial position as a function of the rock physics variables at the same position: $(m_i^1, m_i^2, m_i^3) = g(r_i^1, r_i^2, \dots, r_i^n)$, where g is the rock physics model. We point out that the model update in Equation 2 is proportional

to $\partial\mathbf{A}/m_i$. To transform to the new parameterization \mathbf{r} , we compute the chain rule

$$\frac{\partial\mathbf{A}}{\partial r_i^j} = \frac{\partial\mathbf{A}}{\partial m_i^1} \frac{\partial m_i^1}{\partial r_i^j} + \frac{\partial\mathbf{A}}{\partial m_i^2} \frac{\partial m_i^2}{\partial r_i^j} + \frac{\partial\mathbf{A}}{\partial m_i^3} \frac{\partial m_i^3}{\partial r_i^j}, \quad (5)$$

for each of $j = (1, 2, \dots, n)$. Given the rock physics model g , so that the partial derivatives of \mathbf{m} with respect to \mathbf{r} can be derived, through Equation 5 we can move to a new one in which the vector \mathbf{r} is updated.

Hu et al. (2021, 2022a) illustrate the main advantages of this approach: 1) it allows examination of any rock physics property that has a well-defined relationship with elastic parameters; 2) it shares the same numerical structure as the conventional FWI, and 3) with a suitable initial model, the method exhibits higher prediction accuracy than conventional two-step approaches, in which the elastic properties are first estimated, followed by rock physics properties.

FIELD DATA INVERSION

The inversion results we present here use the data of source line 1 pre-processed by Eaid et al. (2021a). The source line 1 includes shot points 1101-1197 for offsets of 480 meters east and west of the observation well 2. We use 64 shots with both accelerometer and DAS data recorded. The accelerometers were deployed from surface to the bottom of well at 324.2 m depth. Each shot record is converted from the time domain to the frequency domain through a temporal Fourier transform. The inversion is computed over 5 frequency bands using a multiscale approach (Bunks et al., 1995), with each band consisting of 6 equally spaced frequencies. The minimum frequency we use is 10 Hz, which was found to be the lowest frequency at which the ratio of seismic signal to noise was acceptable, and the maximum frequency is 25 Hz, which was limited by the computational costs of moving to the smaller finite-difference grid spacing necessary for higher frequencies (Keating et al., 2021). The initial model is a 1D model built from smoothed well logs of the injection well.

Elastic FWI + Bayesian rock physics inversion

The three-parameter elastic FWI result is shown in Figure 3. This result has several positive features: 1) the model shows efficient update from the initial one, while maintaining the overall trend of each parameter with depth; 2) the model updates are largely layer-like, but exhibit some degree of heterogeneity in the horizontal direction; 3) the inverted parameter values remains in the variation range of the well-log data. 4) unlike previous result which is based on single-parameter inversion, the three models are exempt from having exactly the same structure.

In Figure 4, the measured data of shot 1168 and the corresponding modeled data simulated from the initial model and the inverted model are plotted. The measured data are normalized for source-receiver pair, to prevent under-emphasizing measurements from deeper in the model (Keating et al., 2021). In order to compare these re-scaled data to our simulated data in the FWI procedure, the modeled data are also scaled in a similar way. The result accurately reproduces the measured data. However, we note that much of the data

residuals are eliminated by updating the effective source, or equivalently by changing the modeling of wave propagation through the near-surface.

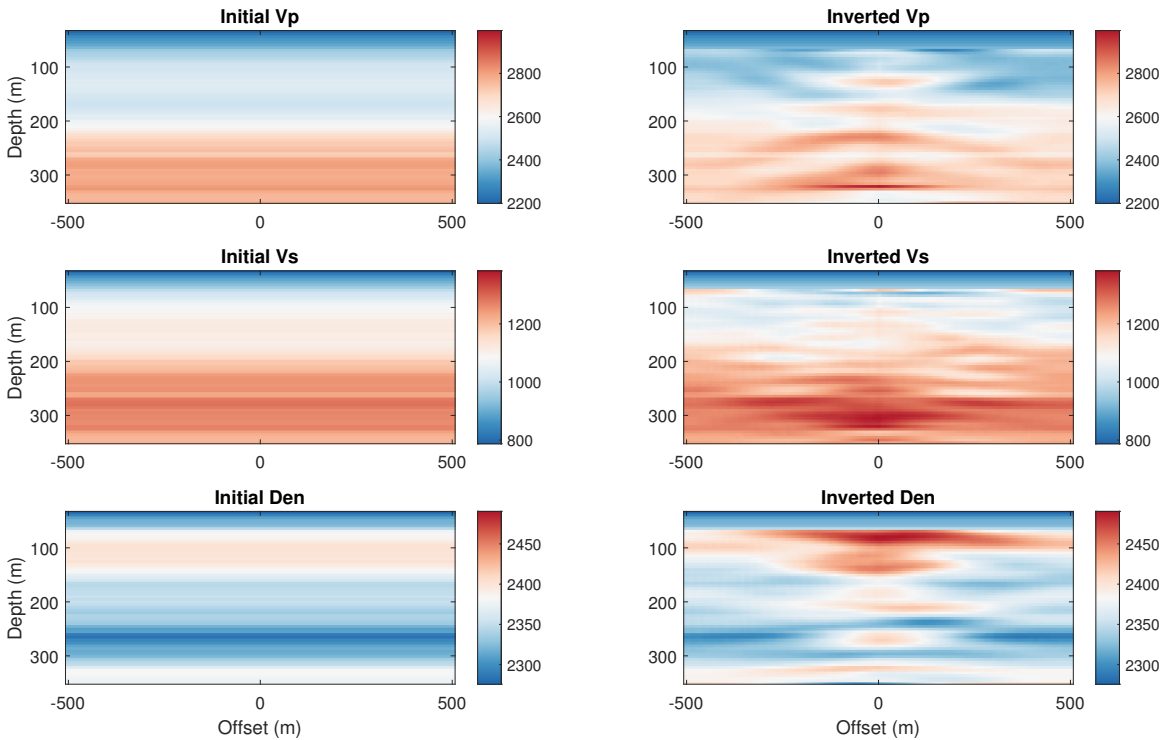


FIG. 3. Initial and inverted models of P-wave velocity, S-wave velocity, and density.

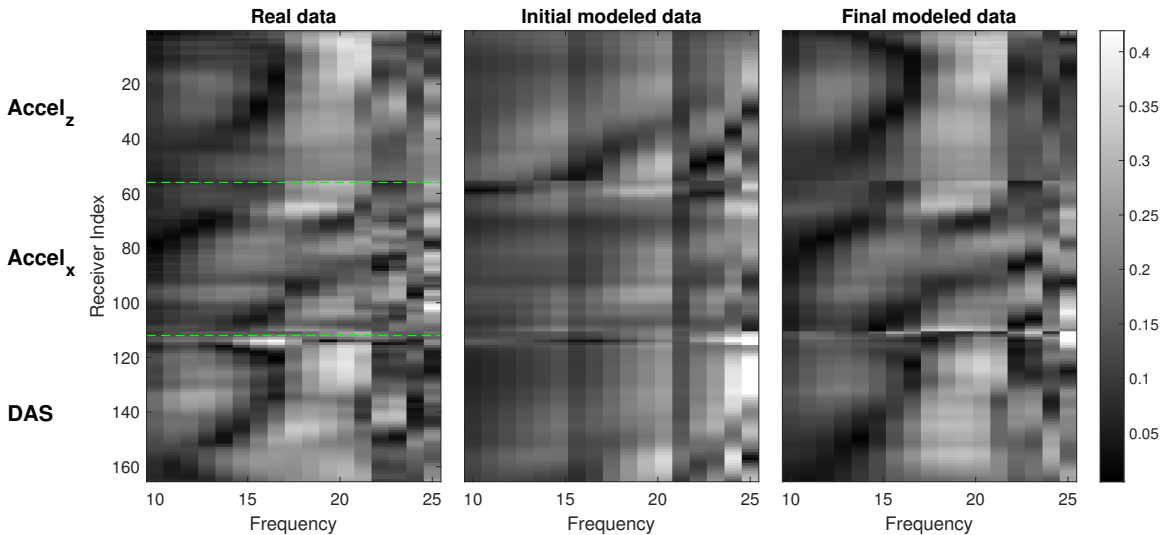


FIG. 4. Comparison between the measured data, the data simulated from the initial model, and the data simulated from the inverted model. The data corresponds to shot 1168. The absolute value of the frequency-domain data is used.

We next use the inverted elastic model as input data to estimate the model of rock properties, based on the rock physics relations built at the injection well (Hu et al., 2022b).

In this application, because the the nonlinearity of the rock physics relations are not strong and the well-log data of the rock physics variables are approximately Gaussian distributed (Figure 5), we adopt a Bayesian linearized inversion method (Grana, 2016). The main advantage of this method is the small computational cost due to the analytical solution given by the linearization of the forward operator and the Gaussian assumption of the prior model. In a companion report, we provide details for the rock physics aspects of the well-log data and the formulation of the inverse problem.

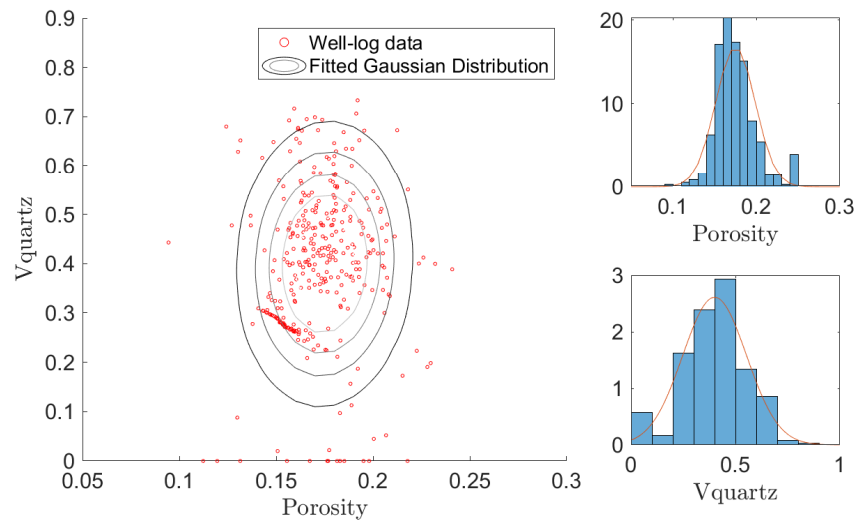


FIG. 5. Gaussian distribution fitted to the well-log data of porosity and quartz content.

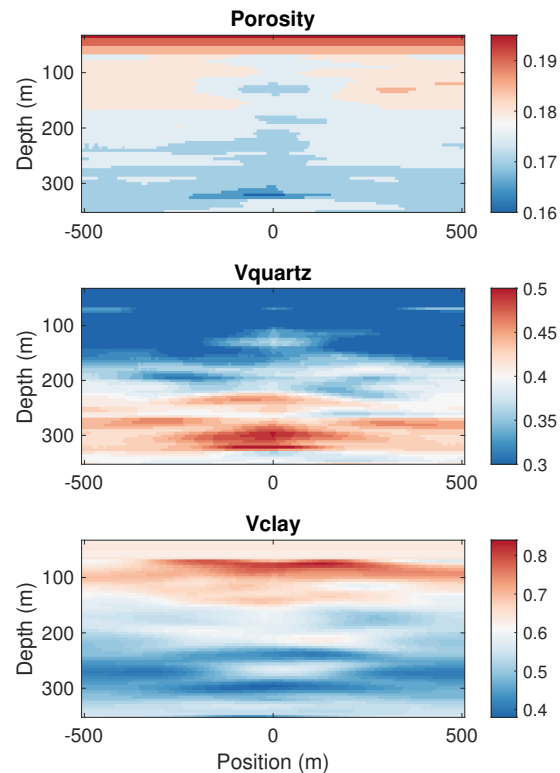


FIG. 6. Bayesian rock physics inversion result: porosity, quartz content, and clay content.

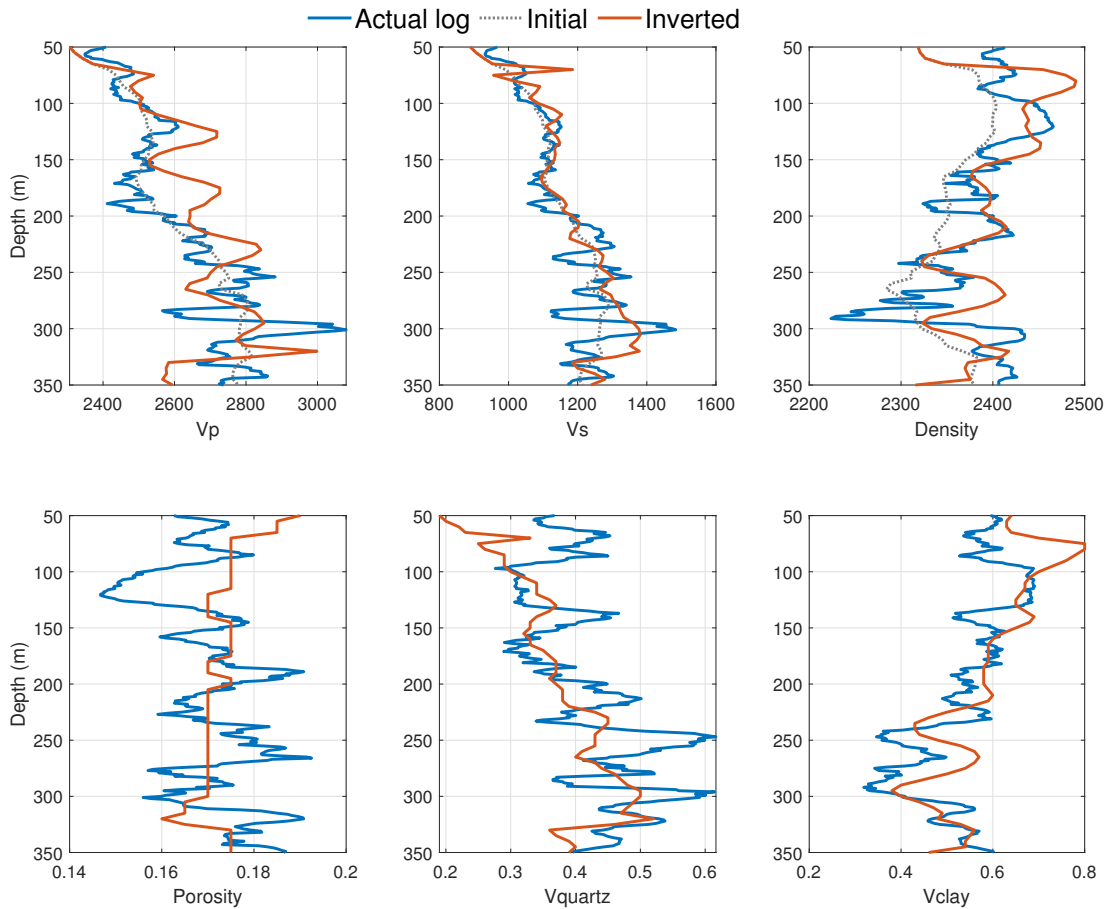


FIG. 7. Results of elastic FWI and Bayesian rock physics inversion at an offset of 20 m. The blue curves are the actual logs (slightly smoothed), the gray curves are the initial models, and the red curves are the inverted models.

Here we apply the Bayesian approach to the 2D case. The inversion result is shown in Figure 6. Although the estimated parameter values are meaningful, the massive "blocky" appearances exhibited on the porosity model and the shallow intervals of the quartz content model are undesirable. In Figure 7, the profiles plotted through the recovered models are summarized. The S-wave velocity, density, and clay content models correlate strongly to the log data, whereas the matches between the P-wave velocity, porosity, and quartz content and their logs are poor.

Direct rock physics FWI

We next repeat the inversion of seismic data using the direct rock physics FWI approach. One of the advantages of this approach is that it allows elastic attributes to be jointly output with rock physics properties. The recovered elastic and rock property models are summarized in Figure 8. Compared with the results of two-step inversion, this result has the following advantages: 1) it has a higher resolution; 2) it shows greater consistency between the elastic and rock property models; 3) it matches more closely the well-log data.

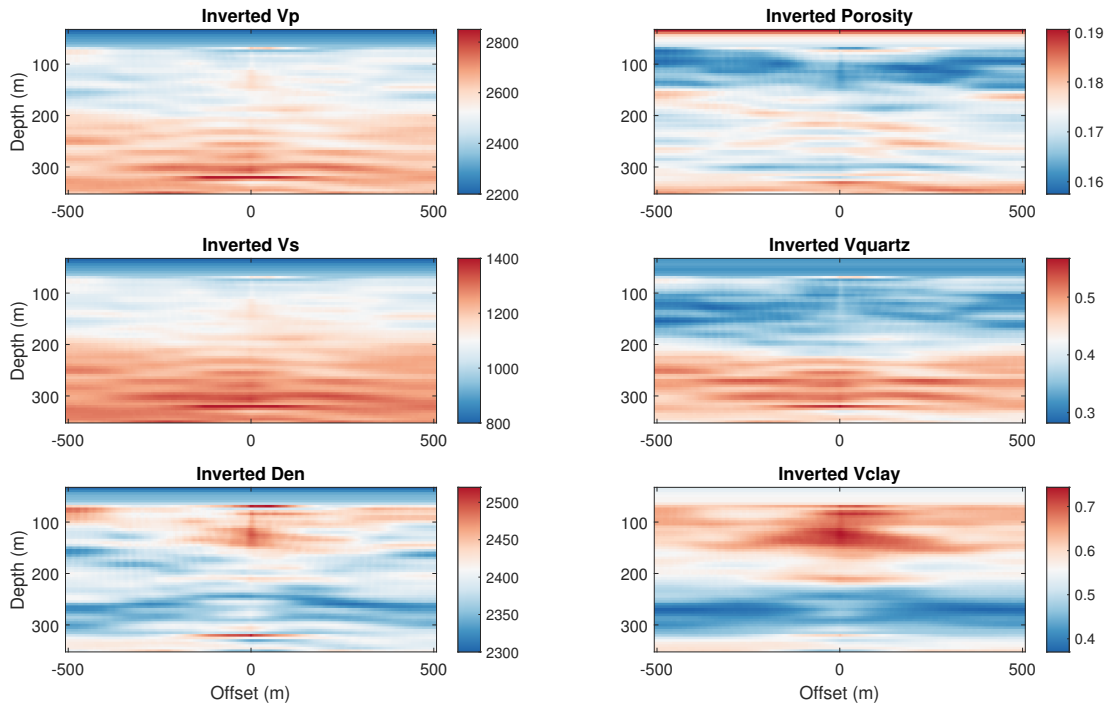


FIG. 8. Recovered elastic and rock property models with direct rock physics FWI.

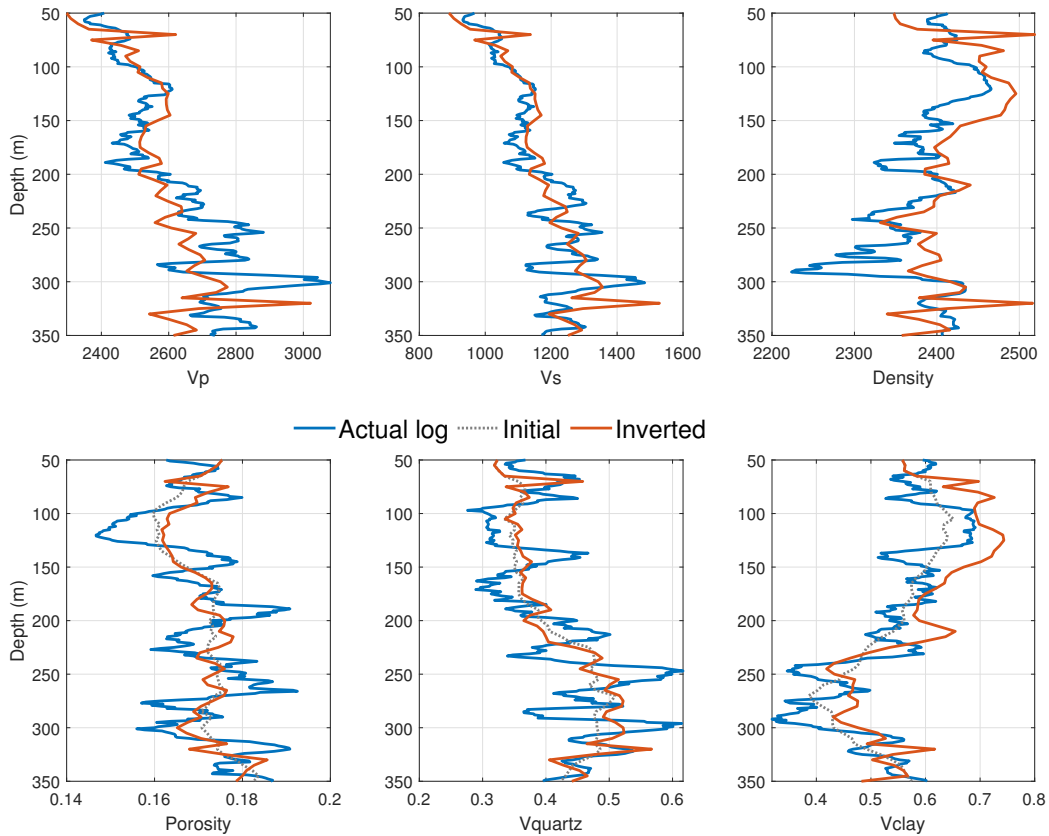


FIG. 9. Results of direct rock physics FWI at an offset of 20 m. The blue curves are the actual logs (slightly smoothed), the gray curves are the initial models, and the red curves are the inverted models.

CONCLUSIONS

In this report, we focus on using the technology of full-waveform inversion (FWI) to reconstruct elastic and reservoir property models from the 2018 CMC VSP survey. The key strategies we apply to the field data include the effective source method, the inclusion of DAS data in FWI, and the FWI framework which allows for direct updating of rock properties. The subsurface model obtained from this survey can be used to support further time-lapse analysis, e.g., reduce the uncertainty in predicting CO₂ distribution during injection and migration.

ACKNOWLEDGMENTS

We thank the sponsors of CREWES for continued support. This work was funded by CREWES industrial sponsors and NSERC (Natural Science and Engineering Research Council of Canada) through the grant CRDPJ 543578-19. The data were acquired through a collaboration with Carbon Management Canada. The first author was partially supported by a scholarship from the SEG Foundation.

REFERENCES

- Bunks, G., Saleck, F. M., Zaleski, S., and Chavent, G., 1995, Multiscale seismic waveform inversion: *Geophysics*, **60**, No. 5, 1457–1473.
- Eaid, M., Keating, S., and Innanen, K., 2021a, Processing of the 2018 CaMI VSP survey for full waveform inversion: *CREWES Research Reports*, **33**, No. 8.
- Eaid, M., Keating, S., and Innanen, K., Innanen, 2021b, Full waveform inversion of DAS field data from the 2018 CaMI VSP survey: *CREWES Research Reports*, **33**, No. 7.
- Eaid, M. V., Keating, S. D., and Innanen, K. A., 2020, Multiparameter seismic elastic full-waveform inversion with combined geophone and shaped fiber-optic cable data: *Geophysics*, **85**, No. 6, R537–R552.
- Grana, D., 2016, Bayesian linearized rock-physics inversion: *Geophysics*, **81**, No. 6, D625–D641.
- Hu, Q., Grana, D., and Innanen, K. A., 2022a, Feasibility of seismic time-lapse monitoring of CO₂ with rock physics parameterized full waveform inversion: *Geophysical Journal International*: accepted for publication.
- Hu, Q., Innanen, K., Macquet, M., and Lawton, D., 2022b, Rock physics analysis of cami.frs well-log datas: *Geoconvention*.
- Hu, Q., Keating, S., Innanen, K. A., and Chen, H., 2021, Direct updating of rock-physics properties using elastic full-waveform inversion: *Geophysics*, **86**, No. 3, MR117–MR132.
- Keating, S., Eaid, M., and Innanen, K., 2021, Full waveform inversion of VSP accelerometer data from the CaMI field site: *CREWES Research Reports*, **33**, No. 28.
- Keating, S., and Innanen, K., 2020, Simultaneous full waveform inversion for sources and anelastic models: *CREWES Research Reports*, **32**.
- Lawton, D. C., Osadetz, K. G., and Saeedfar, A., 2017, Ccs monitoring technology innovation at the CaMI field research station, alberta, canada, *in* EAGE/SEG Research Workshop 2017, European Association of Geoscientists & Engineers, cp–522.
- Nocedal, J., and Wright, S. J., 1999, *Numerical optimization*: Springer.